Acta Biomaterialia 71 (2018) 339–350

Contents lists available at ScienceDirect

Acta Biomaterialia

journal homepage: www.elsevier.com/locate/actabiomat

Full length article

Recovery of low volumes of wear debris from rat stifle joint tissues using a novel particle isolation method

J. Patel [a,*], S. Lal [a], K. Nuss [b], S.P. Wilshaw [d], B. von Rechenberg [b], R.M. Hall [c], J.L. Tipper [a,c]

[a] Faculty of Biological Sciences, University of Leeds, UK
[b] Musculoskeletal Research Unit, University of Zürich, Switzerland
[c] School of Mechanical Engineering, University of Leeds, UK
[d] School of Pharmacy and Medical Sciences, University of Bradford, UK

ARTICLE INFO

Article history:
Received 12 November 2017
Received in revised form 15 February 2018
Accepted 19 February 2018
Available online 2 March 2018

Keywords:
Silicon nitride
Cobalt chromium
Titanium
Particle isolation
Wear
Total joint replacement

ABSTRACT

Less than optimal particle isolation techniques have impeded analysis of orthopaedic wear debris *in vivo*. The purpose of this research was to develop and test an improved method for particle isolation from tissue. A volume of 0.018 mm^3 of clinically relevant CoCrMo, Ti-6Al-4V or Si_3N_4 particles was injected into rat stifle joints for seven days of *in vivo* exposure. Following sacrifice, particles were located within tissues using histology. The particles were recovered by enzymatic digestion of periarticular tissue with papain and proteinase K, followed by ultracentrifugation using a sodium polytungstate density gradient. Particles were recovered from all samples, observed using SEM and the particle composition was verified using EDX, which demonstrated that all isolated particles were free from contamination. Particle size, aspect ratio and circularity were measured using image analysis software. There were no significant changes to the measured parameters of CoCrMo or Si_3N_4 particles before and after the recovery process (KS tests, $p > 0.05$). Titanium particles were too few before and after isolation to analyse statistically, though size and morphologies were similar. Overall the method demonstrated a significant improvement to current particle isolation methods from tissue in terms of sensitivity and efficacy at removal of protein, and has the potential to be used for the isolation of ultra-low wearing total joint replacement materials from periprosthetic tissues.

Statement of Significance

This research presents a novel method for the isolation of wear particles from tissue. Methodology outlined in this work would be a valuable resource for future researchers wishing to isolate particles from tissues, either as part of preclinical testing, or from explants from patients for diagnostic purposes. It is increasingly recognised that analysis of wear particles is critical to evaluating the safety of an orthopaedic device.

1. Introduction

Adverse tissue reactions to wear debris, which may lead to aseptic loosening, are one of the most common causes of total hip replacement (THR) revision [1]. Aseptic loosening remains the most cited reason for THR revision, accounting for 51% of single-stage revisions, while adverse reactions to particulate wear debris account for 10.8% of single-stage revisions [1]. However, the extent of adverse reactions to wear debris is likely to be underestimated, as this was not an option on the revision report forms in the early phase of the National Joint Registry. Several reasons for revision are often given and categories are not mutually exclusive; aseptic loosening and other cited reasons including pain (22.0% of single-stage THR revisions) and lysis (15.6%) are often the result of reactions to wear debris [2,3]. Device failure may be due to a combination of mechanical failure, resulting in high wear, and adverse responses to the wear particles, due to use of potentially unsafe materials. Assessing the biocompatibility of wear debris is therefore crucial to preventing unsafe devices, such as several recalled metal-on-metal THRs, from reaching the market [4]. This is reflected in the publication of recent FDA guidelines [5] for the

* Corresponding author.
E-mail address: mnjpa@leeds.ac.uk (J. Patel).

https://doi.org/10.1016/j.actbio.2018.02.030
1742-7061/

biological evaluation of medical devices, which requests the preclinical assessment of wear debris, including geometric and/or physicochemical properties, specifically in relation to potential biological hazards due to mechanical failure, such as excess wear debris produced as a result of coating delamination. It is thus likely that there will be an increased interest in analysis of wear particles, which may require the use of particle isolation techniques from serum, synovial fluid or tissue.

Particle isolation and subsequent characterisation requires removal of protein and other contaminants such as lipids [6]. Treatment using strong acids or bases has been effectively used to solubilise tissue and facilitate particle extractions. Such protocols have included sodium hydroxide [7–11], potassium hydroxide [12–14] and nitric acid [15–17]. The acids or bases were used at high concentrations from 4 M to 12 M and for one to five days for formalin-fixed tissue, most often at 65 °C. Other studies have isolated metal and ceramic particles using mixed enzymatic and acid/base digestion [18–20]. Although chemical treatment using acids or bases is more efficient than enzymatic tissue digestion [21], acids and bases damage metal particles [22], and thus have been predominantly used to isolate polyethylene particles. Previous studies have used papain and proteinase K to digest periprosthetic tissue to isolate metal particles, with subsequent centrifugation to remove proteins [23], a method which was used and adapted in several later studies for either serum or tissue digestion [22,24,25]. However, such methods involved high temperature stages such as boiling samples in sodium dodecyl sulphate (SDS), which may be overly destructive to recent orthopaedic materials such as silicon nitride (Si_3N_4), which has dissolution properties. Furthermore, the method detailed in the ISO standard for metal particle isolation from tissue [26] requires the use of a tissue homogeniser which could affect large particles and employs multiple washes at relatively low centrifugation speeds of 16,000 RCF (relative centrifugal force) for only ten minutes, which could be insufficient to sediment certain particles. The method could therefore lead to particle loss, making it unsuitable for the recovery of low particle volumes. Due to such disadvantages, particle isolation is not always performed in practice. Further drawbacks of previous methods have included the need for expensive equipment and the length of time required to perform the experiments, a lack of any demonstrated technique sensitivity (as defined by the minimum initial volume of particles that could be successfully extracted from a tissue sample), unsatisfactory results due to protein or bacterial contamination or the presence of extraneous impurities. Many of the methods also did not establish whether use of the isolation method caused any significant changes to particle measurements.

Although several recent publications have provided updated methods for isolating low-wearing materials from serum with proven sensitivity [27,28], such studies have not considered the isolation of particles from tissue, which can be useful when performed on periprosthetic tissue from around explants for diagnostic purposes. The method described by [28] to isolate Si_3N_4 particles from wear simulator serum using density gradient ultracentrifugation with novel sodium polytungstate gradients demonstrated no detectable particle loss at key stages of the procedure, and no detectable changes to particle size or morphology. The method is relatively quick to perform (the protocol requires approximately four days), is cost effective and does not require specialist equipment, making it an attractive technique.

The overall aim of this research study was to produce an improved method for the isolation of wear particles from tissue, using enzymatic digestion and sodium polytungstate density gradients, and test the method in a small animal model on a range of materials.

2. Materials and methods

2.1. Details of the particles employed in the study

Three clinically relevant materials were used in this study: silicon nitride (Si_3N_4), a ceramic material which has been used as an orthopaedic bearing material in cervical spacers and spinal fusion devices and which is currently being investigated as a potential joint replacement coating, cobalt chromium molybdenum alloy (CoCrMo) and titanium aluminium vanadium alloy (Ti-6Al-4V), both of which have been used extensively in various orthopaedic devices for several decades and are included here as intended substrate materials for the Si_3N_4 coating. The Si_3N_4 particles used were a commercially available nanopowder (<50 nm, Sigma-Aldrich). Wear debris of CoCrMo and Ti-6Al-4V were generated using a six-station multidirectional pin-on-plate wear simulator using sterile filtered water as a lubricant, as described previously [29]. Aliquots of each of the three particle types were inspected by scanning electron microscopy (SEM) prior to use to ensure that no contamination was present and that the particles were of a clinically relevant size range. Particles were thereafter sterilised by heat treatment at 180 °C for 4 h and sterile stock suspensions of 0.9 $mm^3 \cdot mL^{-1}$ of each particle type in phosphate buffered saline were produced. Prior to immediate use, the particle suspensions were vortexed and sonicated for 20 min three times to ensure a homogenous dispersion of particles.

2.2. Animal model

The animal test system used for this study consisted of male Wistar rats, 8–12 weeks old and with weights ranging from 297 to 342 g. Guidelines contained in EU Directive 2010/63/EU for animal experiments were followed [30], and the experiments were authorized by the ethical committee under the licence number 133/2014. The study involved a total of 18 rats, consisting of three material groups (Table 1). Tail marks and subcutaneous transponders were placed on the rats on arrival into the facility and the health of each rat was closely monitored; animals with any visible signs of illness were excluded from the study. The rats were acclimatised for at least eight days prior to the study. Stifle joints were chosen for treatment to allow more accuracy and repeatability compared to injection of the hip joints. Rats were injected in the right stifle joint using a glass Hamilton syringe (23 gauge) with 20 μL of a particle suspension (Si_3N_4, CoCrMo or Ti-6Al-4V), which equated to a dose of 0.018 mm^3 of particles per rat stifle joint. The left stifle joints were not injected and were instead used as untreated control joints. Thereafter rats were monitored daily over a seven day period, at which point animals were euthanised with a rising CO_2 concentration. Excess muscle tissue was removed from the stifle joints taking care not to open the joint compartment. The intact rat stifle joints (both treated and non-treated) were excised, formalin-fixed for a period of 48 h, and stored in 70% (v/v) ethanol.

Table 1
Particles used for injection into rat stifle joints.

Material group*	Details
Si_3N_4	Commercially available nanopowder (<50 nm, Sigma-Aldrich, UK)
CoCrMo (high carbon; >0.2%, [31])	Particles generated by pin-on-plate in house
Ti-6Al-4V	Particles generated by pin-on-plate in house

* Volume of particles injected was 0.018 mm^3 and particles were *in vivo* for a period of seven days for each material group (N = 6).

2.3. Histological analysis of rat stifle joints

Intact stifle joints from three rats from each group were decalcified over five weeks at 37 °C with agitation using concentrated EDTA (12.5% w/v, pH 7), replacing the EDTA every two – three days. The decalcified stifle joints were then dehydrated in ethanol and infiltrated with paraffin wax using a tissue processor. Stifle joints were embedded whole using large embedding moulds. Serial sections of 5 μm were taken from a frontal plane from each sample, adhered to charged glass slides, deparaffinised in 100% xylene and transferred to 100% ethanol. Sections were then rehydrated, stained with haematoxylin and eosin and mounted for observation under normal Köhler illumination.

2.4. Analysis of particles within tissue sections using scanning electron microscopy

Recut sections were deparaffinised, transferred to 100% ethanol, dried at room temperature, coated with carbon to a thickness of approximately 15 nm, and imaged using cold field emission scanning electron microscopy (CFE-SEM; Hitachi SU8230) with a backscattered electron detector, at magnifications up to 5000×. Particles were analysed by energy dispersive X-ray analysis (X-Max EDX system, Oxford, UK) to confirm the composition of the particles; the analysis was performed at a working distance of 15 mm and using a potential of 15 kV.

2.5. Particle isolation

The recovery rate of the particle isolation method detailed in [28], which utilised sodium polytungstate density gradient ultracentrifugation to isolate particles from wear simulator serum, was tested gravimetrically by weighing recovered particles on filters as detailed in [32] to verify the efficacy of using sodium polytungstate gradients. A novel tissue digestion method was developed and optimised as described in [33] to produce an isolation protocol for tissue samples. The protocol was validated in each material by recovering particles from particle-doped tissue samples as detailed in [34] prior to commencing with particle isolation from the injected rat stifle joints.

The remaining three injected stifle joints from each material group, in addition to an untreated contralateral stifle joint were washed three times by filling each sample tube with sterile filtered water and discarding each wash, and approx. 0.15 g (wet weight) of tissues from the ligament of the patella and fat pad were harvested and minced. Samples were digested with gentle agitation at 50 °C with 1.56 mg·mL^{-1} of buffered papain (Sigma-Aldrich, UK), in the presence of 0.1 M HEPES buffer (pH 7.5) and 0.33 M glycine (Sigma-Aldrich, UK), in a sample volume of 3 mL (made up with sterile water). After six hours of digestion at 50 °C, proteinase K stock solution (20 mg·mL^{-1} in 0.5 M HEPES buffer, pH 7.5, containing 3 mM $CaCl_2$) was added to a concentration of 1 mg·mL^{-1} and SDS was added to a concentration of 0.5% (v/v). Digestion was continued at 50 °C with agitation for 16–20 h, after which an additional 150 μL of the 20 mg·mL^{-1} proteinase K stock was added. The addition of 150 μL of proteinase k stock was repeated after six hours. Digestion was completed at 48 h. Digested samples were subjected to density gradient ultracentrifugation on gradients of 2 g·mL^{-1}, 1.6 g·mL^{-1} and 1.2 g·mL^{-1} of sodium polytungstate solution; samples were ultracentrifuged at an average RCF of 202,048 for 4 h. The supernatant was removed from each sample, leaving particles at the bottom of each tube. Addition of filtered water and further ultracentrifugation for 1 h at an average RCF of 154,693 was repeated three times to remove residual SPT. The supernatant was removed from each sample, leaving isolated particles which were collected from the bottom of each tube. Isolated particle samples were sealed with parafilm and stored at −20 °C, before resuspension and filtration for characterisation.

2.6. Particle characterisation

Isolated particles (entire samples) were resuspended by sonication in an ice-cooled water bath for 20 min, vortexing samples every 5 min, and filtered onto 0.015 μm pore size polycarbonate filter membranes. In addition, non-isolated particles, which were not injected and thus not subjected to the isolation process, were also resuspended and filtered for comparison, at volumes of 0.018 mm^3. The filters were dried overnight at room temperature and mounted directly onto aluminium stubs before being coated with iridium to a thickness of 4 nm (Agar Scientific, UK). The filter membranes were then imaged using cold field emission (CFE) SEM (Hitachi SU8230). For Si_3N_4 and CoCrMo particles, images were captured at 2000× and 20,000× magnification to provide an overview of the filter membranes and particle aggregates. In addition, for Si_3N_4 and CoCrMo particles, at least five random fields of view of particle aggregates were captured at 100,000× magnification for particle characterisation. For titanium particles, due to the large particle size range, it was necessary to capture images at magnifications of 100×, 500× and 1000× to enable particle characterisation. Elemental characterisation of the particles was performed as detailed in Section 2.4, at a magnification of approximately 20,000×. The CFE-SEM micrographs of the particles were subsequently analysed using ImageJ (version 1.49), to measure the Feret's diameter (defined as the greatest distance between any two points on the particle boundary), aspect ratio (major particle axis/minor particle axis) and circularity (as given by $4\pi \times \text{area}/[\text{perimeter}^2]$) of the particles. A minimum of 150 Si_3N_4 and 150 CoCrMo particles from each sample were measured in accordance with the standard practice for characterisation of particles [26,35]. A minimum of 100 titanium particles from each sample were also measured.

2.7. Statistics

Isolated Si_3N_4 and CoCrMo particles were compared statistically to non-isolated particles that were not injected into tissue by Kolmogorov-Smirnov tests of each measured parameter (IBM SPSS, v23). In each case, the raw data from 150 isolated particles was compared to the raw data from 150 of the non-isolated particles. This was repeated for each of the three rat samples using three separate control data sets for both material groups.

3. Results

3.1. Histological analysis of rat stifle joints

Particles were not present in non-treated stifle joints and were located toward the frontal part of each injected joint. Particles were observed to have formed deposits within the fat pad (Fig. 1) and were also present in the patella ligament and synovium. Silicon nitride particles were barely visible using light microscopy (Fig. 1A), however Ti-6Al-4V and CoCrMo particles were clearly visible and were dark in appearance (Fig. 1B and C). Cellular reactions accompanied the presence of particles in all three materials groups, and consisted predominantly of neutrophils, macrophages and lymphocytes. A greater response including larger numbers of infiltrating cells and possible necrosis, which was completely absent in the other material groups, was observed in the CoCrMo group (Fig. 1C).

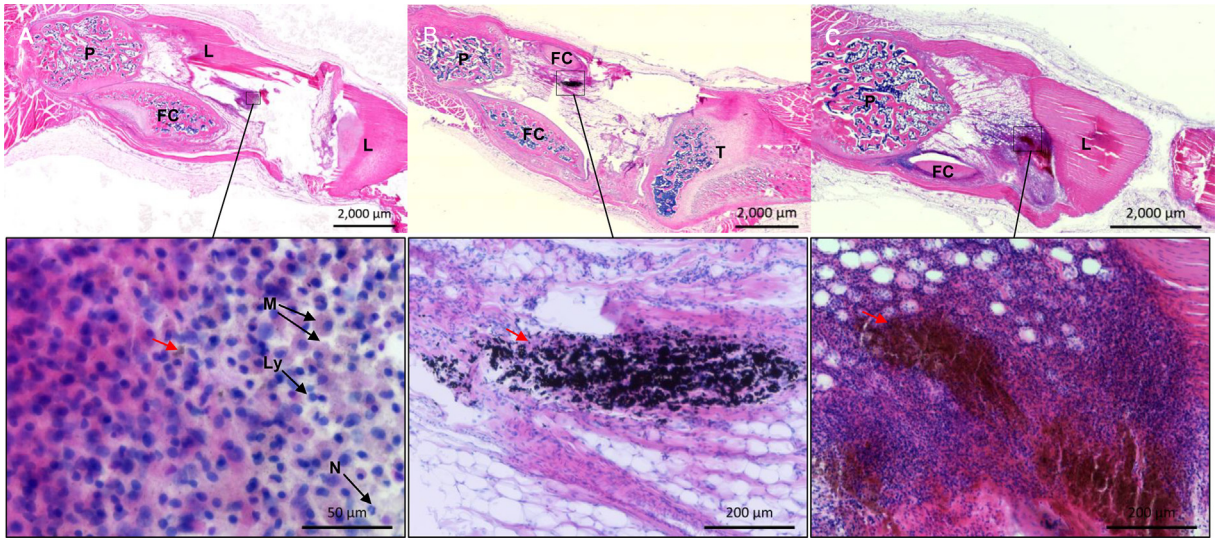

Fig. 1. Histological sections from (A) a Si_3N_4 injected rat stifle joint, (B) a Ti-6Al-4V injected joint, and (C) a CoCrMo injected joint. The joints were embedded in paraffin wax whole, cut from a frontal plane, stained with H&E and viewed under normal Köhler illumination. Areas of inflammation and particle deposition in the fat pad are shown in high magnification beneath; particles are indicated by red arrows and specific cell types are labelled with black arrows. P = patella, FC = femoral condyle, L = ligament, Ly = lymphocyte, M = macrophage, N = neutrophil, T = tibia. (For interpretation of the references to colour in this figure legend, the reader is referred to the web version of this article.)

3.2. Analysis of particles within tissue sections using scanning electron microscopy

Analysis of tissue samples using CFE-SEM did not allow cells to be easily distinguished, and particles appeared to be partially covered by the extracellular matrix; however, particles could be detected within the tissue using back scatter, where they appeared bright against a dark background (Fig. 2). The CFE-SEM analysis of tissue samples showed that the Si_3N_4 particles were aggregated in a similar way to those that were not subjected to *in vivo* exposure (Fig. 2A). Ti-6Al-4V particles were also similar in appearance to Ti-6Al-4V particles that were not subjected to *in vivo* exposure (Fig. 2B). In contrast to CoCrMo particles that were directly filtered for CFE-SEM analysis, the CoCrMo particles within tissue sections were either present as large deposits (Fig. 2C) or dispersed aggregates (Fig. 2D). Elemental analysis confirmed the composition of these particles (Fig. 3), with silicon and nitrogen present in the Si_3N_4 group (Fig. 3A), titanium and aluminium present in the Ti-6Al-4V group (Fig. 3B) and cobalt and chromium present in the CoCrMo group (Fig. 3C). In spectrum analysis, vanadium was also identified exclusively in Ti-6Al-4V particles, and molybdenum was identified

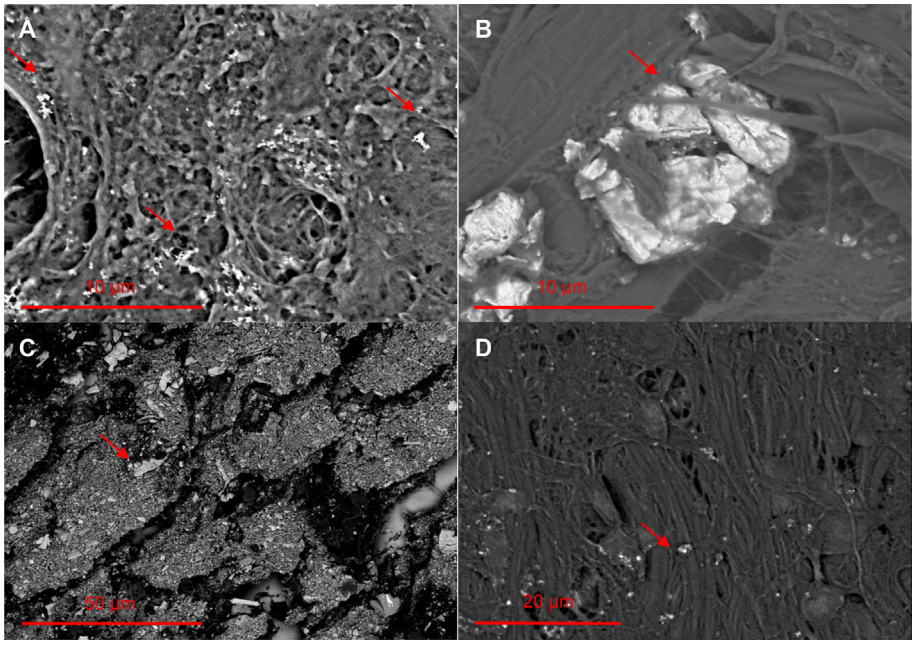

Fig. 2. Images of a whole joint section from (A) a Si_3N_4 injected rat stifle joint, (B) a Ti-6Al-4V injected joint and (C) and (D), a CoCrMo injected joint. The tissue sections were dehydrated in ethanol, carbon coated and imaged by scanning electron microscopy using back scattered electrons, to enable heavier elements to be distinguished by their brighter appearance. Particle aggregates are indicated by red arrows. (For interpretation of the references to colour in this figure legend, the reader is referred to the web version of this article.)

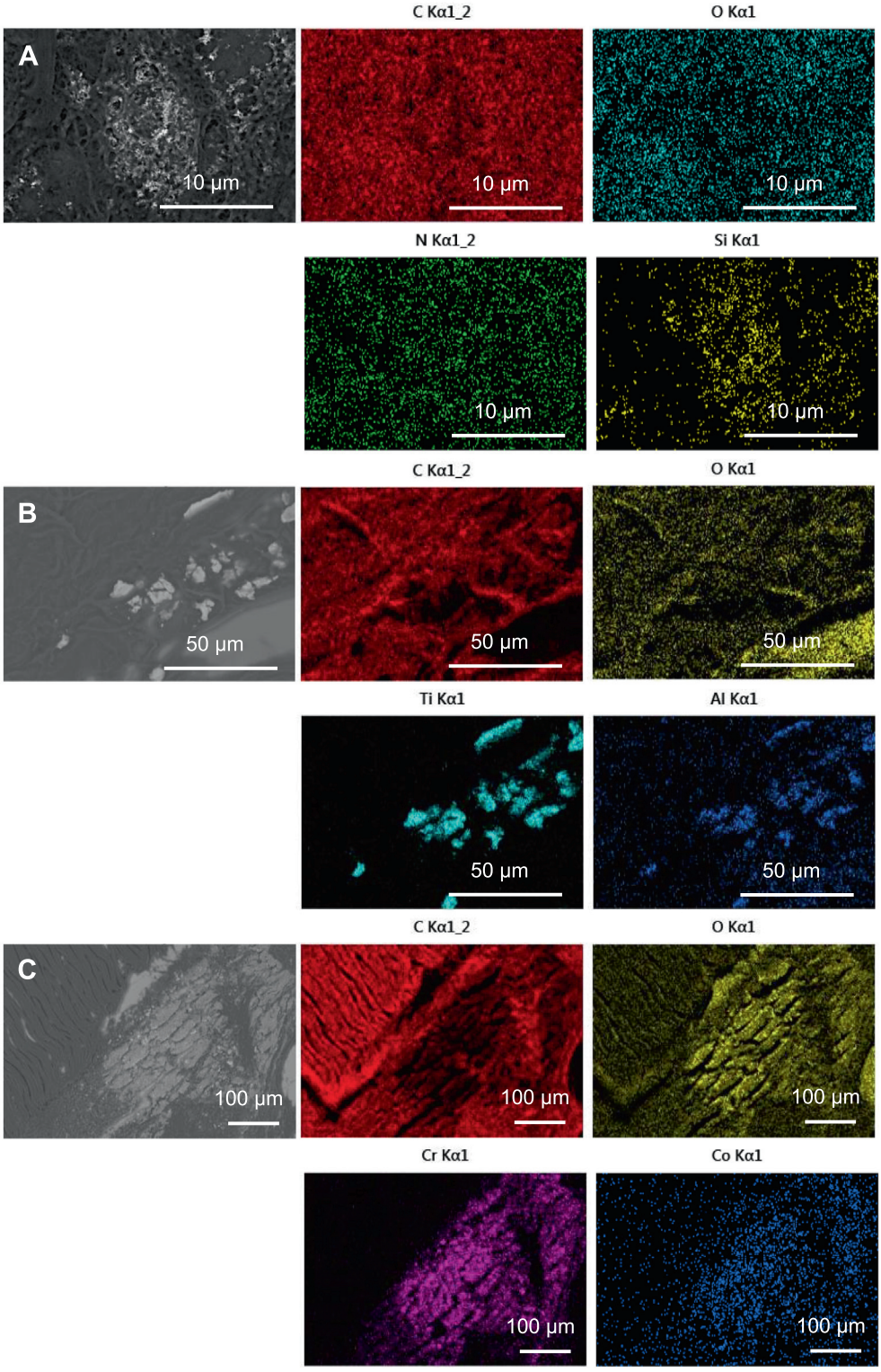

Fig. 3. Elemental analysis of tissue sections from (A) a Si_3N_4 injected rat stifle joint, (B) a Ti-6Al-4V injected joint, and (C) a CoCrMo injected joint. The sections were dehydrated in ethanol, carbon coated and imaged by scanning electron microscopy with back scattered electrons (grayscale images); elements were detected by energy dispersive X-ray spectroscopy to produce corresponding elemental maps of each imaged area (coloured images). Carbon, oxygen and nitrogen were ubiquitous in the tissue. Signals originating from the glass slide were omitted. (For interpretation of the references to colour in this figure legend, the reader is referred to the web version of this article.)

exclusively in CoCrMo particles. CoCrMo particles appeared to be oxidized, as significant oxygen signals were detected in the CoCrMo particles (Fig. 3C); this was not apparent in Si_3N_4 or Ti-6Al-4V particles.

3.3. Particle isolation

The average recovery rate obtained from serum samples doped with 1 mm^3 of Si_3N_4 particles was 89.6% ± 7.1% SD [32]. Tissue digestion optimisation experiments showed that the use of papain, glycine in the buffer, and frequent proteinase K enzyme replenishment were required to efficiently digest tissue proteins [33]. Validation of the method in tissue samples doped with 0.0025 mm^3 of particles per sample demonstrated that the protocol used had no effect on particle size or morphologies for any of the materials, and was effective at very low particle doses [34].

Digested rat tissue samples were visibly homogeneous, containing no large pieces of undigested tissue, and during the isolation process the proteins in each sample formed a faint band within the upper density gradient layers, enabling separation from particles. The commercial silicon nitride particles (<50 nm) and titanium particles that were used in the study did not form a visible pellet, however CoCrMo particles formed a hard pellet following density gradient ultracentrifugation. For each material group, particles were isolated from every tissue sample, and were absent from the contralateral stifle control sample, demonstrating that particles were not present in the tissues as a result of contamination. In every case, isolated particles were visibly similar to particles not subjected to the recovery process (Figs. 4–6). The Si_3N_4 particles were observed as aggregates of approximately 0.2–2 μm in size distributed across the filter membrane (Fig. 4). Titanium particles were highly dispersed on the membrane and showed no aggregation characteristics, in contrast to the Si_3N_4 particles (Fig. 5). The CoCrMo particles formed small aggregates of a similar size to the Si_3N_4 aggregates.

Elemental analysis was used to confirm the composition of the particles post-isolation (Fig. 7), with similar results to those obtained from the elemental analysis of tissue sections detailed in Section 3.2, as the same elements were present within each material (Table 2). The oxidation detected in CoCrMo particles was also apparent post-isolation and was also detected to a lesser extent in Si_3N_4 and Ti-6Al-4V particles post-isolation (Fig. 7C). Furthermore, traces of tungsten were detected by spectrum analysis on the CoCrMo particles post-isolation, which likely originated from the sodium polytungstate gradient. No other contaminating elements were detected.

Isolated and non-isolated particles had similar size distributions, average particle sizes, aspect ratios and circularities (Fig. 8). For both Si_3N_4 and CoCrMo particles, sizes ranged from 10 to 60 nm (Fig. 8A and B), though the CoCrMo size distribution was more positively skewed. Si_3N_4 particles had a modal particle size of 20–30 nm, while CoCrMo particles had a modal size of 10–20 nm. Titanium particles exhibited a broader size distribution from 0.1 to 100 μm, with a modal particle size of 10–15 μm (Fig. 8C). Based on the measured parameters (Fig. 8D), and with reference to [35] and [26] the Si_3N_4 and CoCrMo particles were considered spherical. Titanium particles were considered oval or irregular in shape. Statistical analysis of the geometric measurements of the Si_3N_4 and CoCrMo particles confirmed that the differences in particle size distributions and morphologies between isolated and non-isolated particles were not significant (KS test, $p > 0.05$). Titanium particles were not analysed statistically, since it was not feasible to measure the minimum of 150 particles recommended in [26].

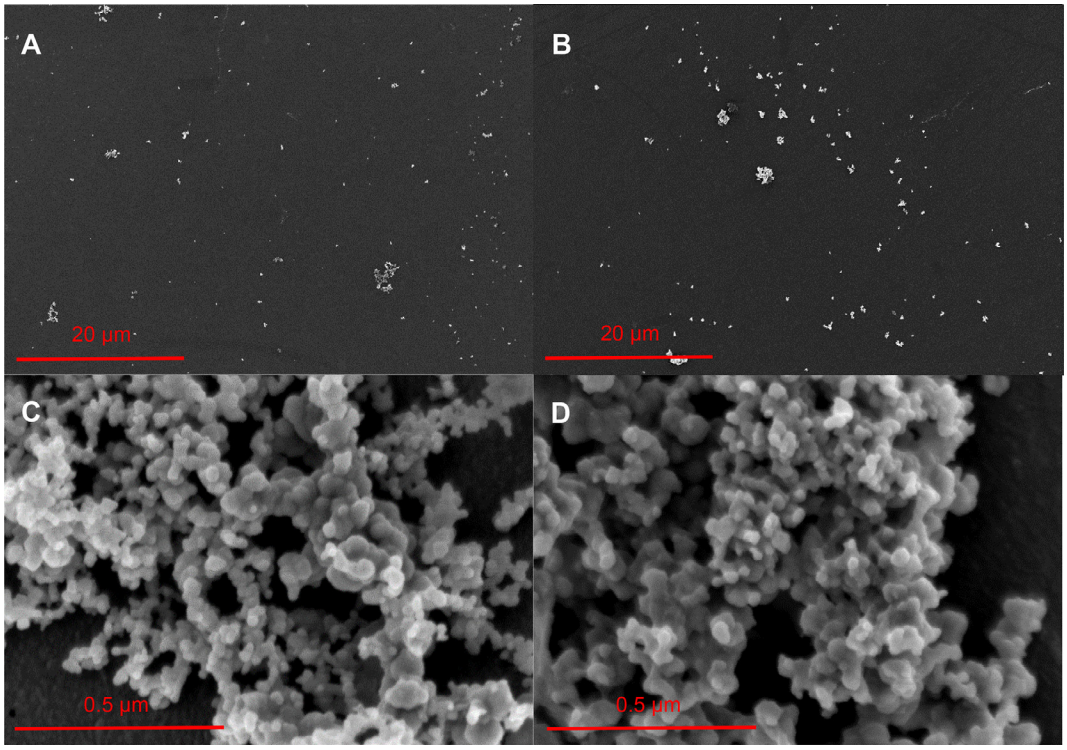

Fig. 4. Si_3N_4 particles imaged by scanning electron microscopy. (A) Particles not injected or subjected to the recovery procedure, at a low magnification. (B) Particles following isolation from an injected rat stifle joint, at the seven-day *in vivo* time point, at a low magnification. (C) The same particles as (A) at a high magnification. (D) The same particles as (B) at a high magnification.

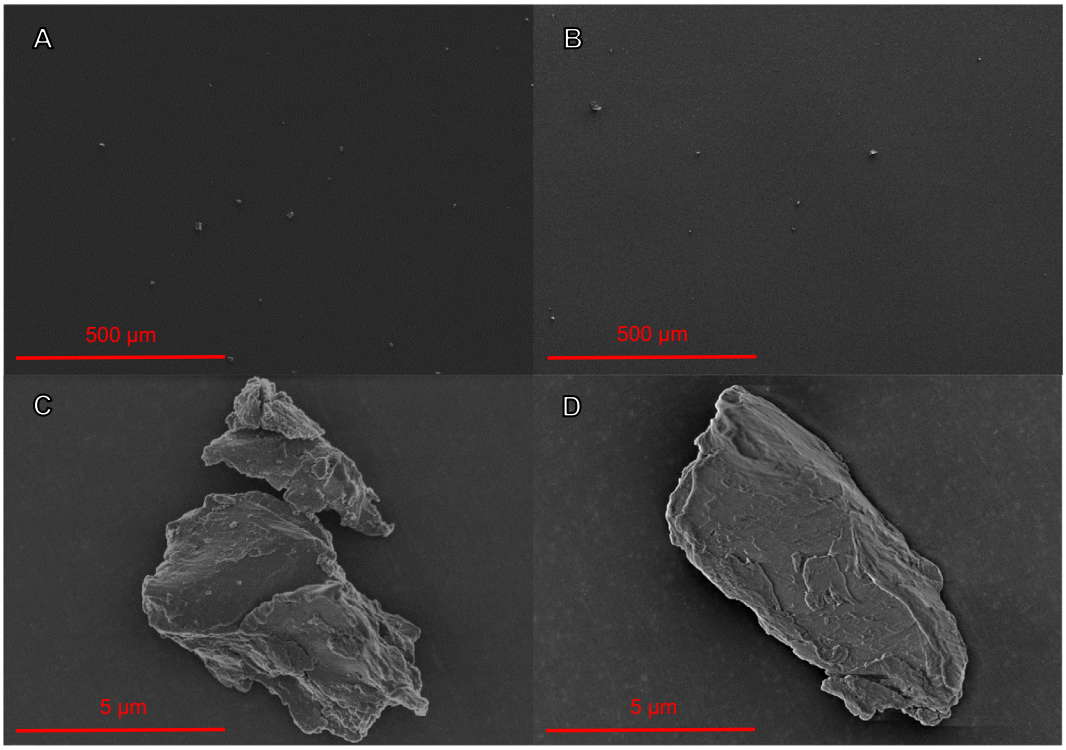

Fig. 5. Ti-6Al-4V particles imaged by scanning electron microscopy. (A) Particles not injected or subjected to the recovery procedure, at a low magnification. (B) Particles following isolation from an injected rat stifle joint, at the seven-day *in vivo* time point, at a low magnification. (C) The same particles as (A), at a high magnification. (D) The same particles as (B) at a high magnification.

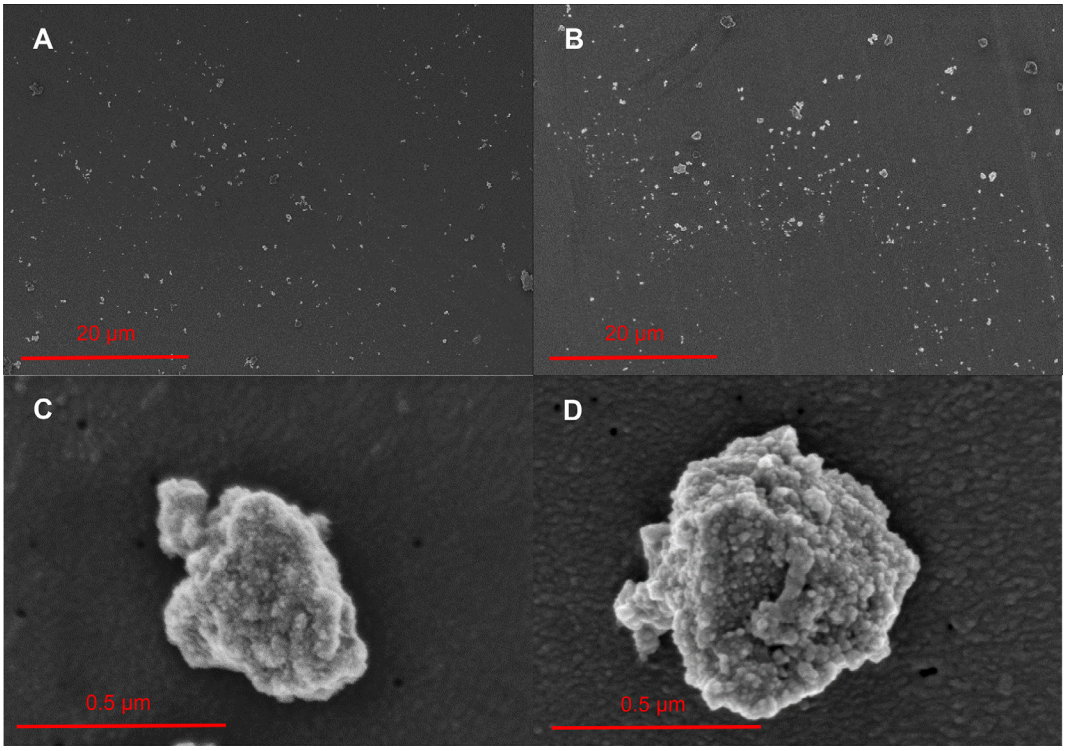

Fig. 6. CoCrMo particles imaged by scanning electron microscopy. (A) Particles not injected or subjected to the recovery procedure, at a low magnification. (B) Particles following isolation from an injected rat stifle joint, at the seven-day *in vivo* time point, at a low magnification. (C) The same particles as (A) at a high magnification. (D) The same particles as (B) at a high magnification.

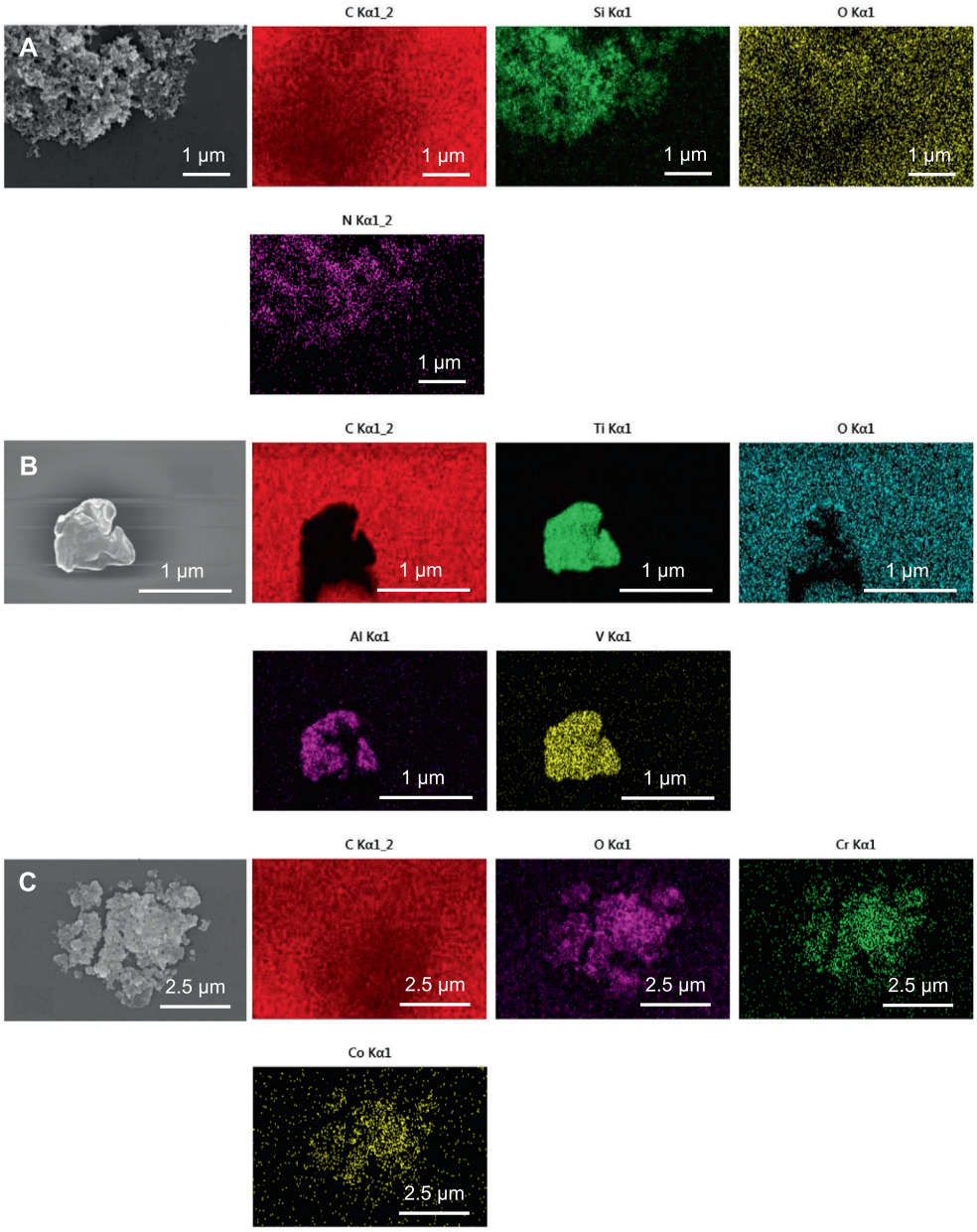

Fig. 7. Elemental analysis of particles isolated from (A) a Si_3N_4 injected rat stifle joint, (B) a Ti-6Al-4V injected joint and (C) a CoCrMo injected joint. The isolated particles were filtered directly onto polycarbonate membranes, iridium coated and imaged by scanning electron microscopy with back scattered electrons (grayscale images); elements were detected by energy dispersive X-ray spectroscopy to produce corresponding elemental maps of each imaged area (coloured images). Carbon signals originated from the polycarbonate membrane. (For interpretation of the references to colour in this figure legend, the reader is referred to the web version of this article.)

Table 2
Elemental components of particles detected by energy dispersive X-ray spectroscopy before and after particle isolation.

Elements present in detectable quantities*	Si_3N_4 particles		Ti-6Al-4V particles		CoCrMo particles	
	Within injected rat tissue	After isolation from tissue	Within injected rat tissue	After isolation from tissue	Within injected rat tissue	After isolation from tissue
Aluminium			X	X		
Cobalt					X	X
Chromium					X	X
Molybdenum					X	X
Nitrogen	X	X				
Oxygen		X		X	X	X
Silicon	X	X				
Titanium			X	X		
Tungsten						X
Vanadium			X	X		

* Elements present in the background (such as iridium from the sputter coating) have been excluded. Silicon and metal elements were not detected in control tissue from an untreated stifle joint.

A

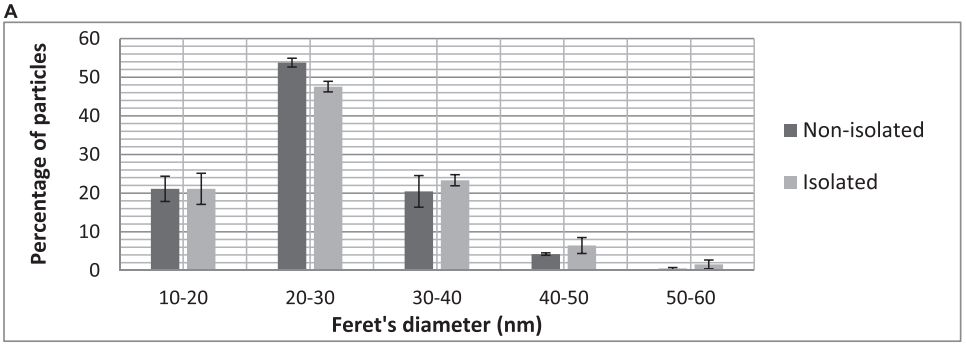

B

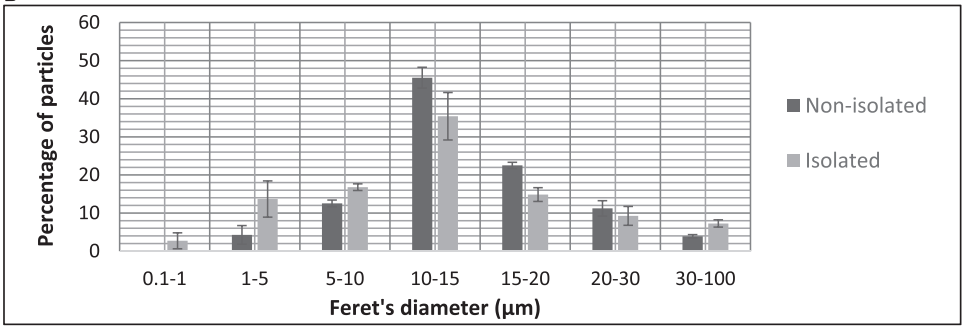

C

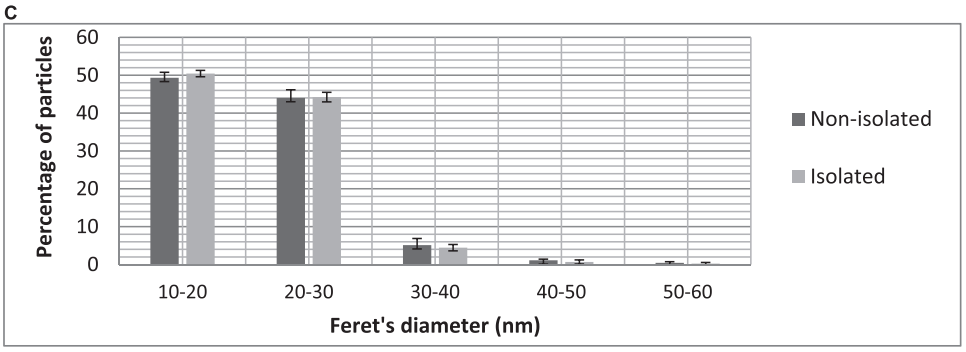

D

Parameter	**SiN Non-Isolated Particles** Mean (N=3) +/- SD	**SiN Isolated Particles** Mean (N=3) +/- SD	**Titanium Non-Isolated Particles** Mean (N=3) +/- SD	**Titanium Isolated Particles** Mean (N=3) +/- SD	**CoCr Non-Isolated Particles** Mean (N=3) +/- SD	**CoCr Isolated Particles** Mean (N=3) +/- SD
Feret's diameter	**25.85** +/- 0.94 nm	**27.20** +/- 1.14 nm	**14.86** +/- 7.71 µm	**13.99** +/- 10.95 µm	**20.92** +/- 0.14 nm	**20.59** +/- 0.27 nm
Aspect ratio	**1.21** +/- 0.02	**1.19** +/- 0.01	**1.56** +/- 0.42	**1.71** +/- 0.58	**1.27** +/- 0.02	**1.24** +/- 0.02
Circularity	**0.92** +/- 0.00	**0.92** +/- 0.00	**0.77** +/- 0.11	**0.67** +/- 0.14	**0.90** +/- 0.01	**0.91** +/- 0.00

Fig. 8. Size distributions and average particle measurements for pristine, non-isolated particles, and particles isolated from injected rat stifle joints, for (A) Si_3N_4 (B) Ti-6Al-4V and (C) CoCrMo material groups, and (D) average particle parameters for each material. Error bars give standard deviation (±).

4. Discussion

This study developed novel methodology that successfully isolated low volumes of micronscale and nanoscale particles from tissue, without discrimination to particle size or morphology, from a total of nine different animal samples. The animals were injected with either Si_3N_4 (N = 3), CoCrMo (N = 3) or Ti-6Al-4V (N = 3), demonstrating that the isolation method is effective in a variety of different materials. Initial particle volumes were 0.018 mm^3, suggesting that the technique is highly sensitive. Particles were demonstrably unchanged by the isolation procedure. Proteins were effectively removed and the isolated particles were relatively pure, and were not irreversibly bound to any surface, so particles isolated using the method have the potential to be used in further studies; for example with nanoparticle-tracking analysis. This study has taken the initial progress made by [28] forward by adapting the isolation process for a new application – the isolation of particles from tissue samples. This has involved changes to the method presented by [28] including sample preparation, the removal of certain stages of the protocol, and optimisation of the digestion protocol specifically for fixed tissue samples. Previously the isolation process had not been tested on micron-scale particles, only nanoscale particles, and had also not been used to isolate titanium particles. The use of an *in vivo* model also enabled

histological analysis of injected particles within tissue sections, scanning electron microscopy and elemental analysis of particles within tissues.

Rats were chosen rather than mice to allow a sufficient dose of particles to be injected and to enable an appropriate amount of tissue to be harvested for particle isolation; in addition, the joints were still small enough for whole-joint histological analysis to be feasible. The volume of injected particles was 0.018 mm^3, which is lower than the volume of particles that would normally be recovered from an explant tissue sample, since the volume of particles per gram of tissue from a failed hip prosthesis has been estimated at 0.37 mm^3 [36]. Failed ceramic-on-ceramic bearings may produce 1–5 mm^3 of wear per year [37]. However, particle concentration in any given explant tissue sample could vary substantially, for example depending on the location from which tissue was extracted, the performance of an implant, and the clearance rate of particles within the tissue. Particle amounts could therefore be extremely low, especially in well-functioning ceramic-on-ceramic bearings which may produce less than 0.5 mm^3 of wear per year *in vivo* [38]. The current method was therefore tested in particle-doped tissue samples at starting volumes as low as 0.0025 mm^3 per sample of tissue [34]. The *in vivo* exposure time of seven days was the maximum time point that could enable protein binding to particles before a large volume of particles would be lost through dissemination. It has previously been shown that following injection of mice stifle joints with nanoscale and micron scale CoCrMo particles, approximately 60–70% of the injected metal was no longer present in the peri-articular tissue after seven days, and particles were found to disseminate via lymph nodes [39]. Samples in this study were formalin-fixed as this is the conventional way to preserve explant samples for biological analysis; subsequent storage of samples in 70% (v/v) ethanol also prevents bacterial contamination of samples. Particles were first located within histological tissue sections with a previously used technique [40] to enable accurate tissue harvesting. Due to the small amount of tissue available from a rat stifle joint, initial tissue masses (wet weight) were 150 mg; however, since larger quantities of tissue are sometimes available from human explant samples, the particle isolation method was also tested on initial tissue masses of 250 mg [34].

Improvements to the isolation method included optimisation of tissue digestion. Glycine was used to achieve complete digestion, as previous research has shown it improves formalin-fixed tissue digestion with proteinase K, possibly by preventing inactivation of the enzyme or protein re-crosslinking, by inactivating the formyl group of formaldehyde [41]. The tissue digestion method was optimised prior to application to the *in vivo* study using cadaveric ovine and porcine capsular tissues [33]. The results of this analysis support the use of glycine and the use of papain for increasing the efficiency of tissue digestion. More frequent enzyme replenishment, rather than larger but less frequent doses were also more effective, possibly due to gradual loss of enzyme activity. During the particle isolation protocol, transfer of samples between tubes was minimised to twice, and any sample tubes were washed with sterile filtered water three times, whilst sonicating, and these washes were added to samples, to prevent particle loss. Previous work has shown minimal particle loss during removal of supernatant following ultracentrifugation [28], and low speed centrifugation steps, which could lead to particle loss, were omitted from the current protocol. It is also worth noting that this method required only four days of processing time (excluding particle characterisation), did not require any specialist equipment, had relatively few stages and was cost effective, making it more efficient to perform then previous methods [24,42]. Since the particle recovery rate of the method would be difficult to accurately assess using an *in vivo* model due to particle dissemination, the recovery rate in particle-doped serum samples was investigated prior to this study gravimetrically [32], and an average recovery rate of 89.6% ± 7.1% (SD) was achieved. This is a similar recovery rate to that reported by [28]. To prevent extraneous particle contamination, where possible all solutions were filtered using 0.02 μm pore-size filters prior to use. To minimise variations in particle aggregation, all particle samples were re-suspended and filtered using the same protocol and to prevent bias during imageJ measurements, images were randomised, and all the particles that were visible in each image were measured. Manual sizing of individual particles was used rather than automatic sizing functions, which may inaccurately define particle boundaries. Scanning electron microscopy (SEM) was chosen rather than transmission electron microscopy (TEM) for particle characterisation to enable the surface characteristics of particles to be analysed. Surface characteristics play a crucial role in how particles interact with proteins and thus in the overall biocompatibility of a material [43].

The CoCrMo and Ti-6Al-4V particles used in this study were similar in size and shape to those retrieved from periprosthetic tissues and those generated by physiological hip simulators [19,24,44–46]. The size and shape of CoCrMo and Ti-6Al-4V particles showed slight variation between the validation study [34] and the rat study. In particular, CoCrMo particles were slightly smaller in the rat study and Ti-6Al-4V particles had a higher average circularity. This may be due to variation between particle generation experiments. The model Si_3N_4 particles used were similar in size to recently published data on nanoscale Si_3N_4 debris produced by a coating applied to a CoCrMo substrate [47], though particles up to a few microns in size were also identified by [47]. The nanoscale silicon nitride particles were also spherical and existed as aggregates of a similar size to those observed in the current study. Measuring the chosen parameters for the particles was important due to their significance to the biological activity of particles. For example, UHMWPE particles in the 0.1–1 μm size range have been found to be more biologically active in terms of osteolytic cytokine release than particles above 1 μm in size, and it was found that particles of a size below approximately 50 nm failed to elicit a pro-inflammatory response in primary cells [48]. Further, based on a murine model involving injected particles, nanoscale and not micronscale CoCrMo particles were genotoxic at 40 weeks *in vivo* [39]. Size-related differences in particle biocompatibility may be due to how readily cells are able to phagocytose particles. Aspect ratio may also affect cellular uptake of particles [49], and UHMWPE particles with a more elongated shape are more inflammatory [50]. Spherical nanoparticles with a circularity of greater than 0.7, when taken up by cells, may have different biological effects than less spherical particles, since particles with rough edges may break through endosomal or lysosomal membranes and thus reside more frequently in cytoplasm [51]. Measuring particle parameters also allows detection of particle dissolution; our results suggest that Si_3N_4 particles may dissolve less quickly *in vivo* than has been previously suggested by simulations of *in vivo* conditions [47], since there were no detectable changes to particle size or shape. Additionally, results suggest that corrosion of particles, which may occur within macrophages, did not affect a significant number of particles within the given time frame.

There were several limitations to the current study. Particle adhesion to the glass syringe may have occurred during injection, and hence there may have been slightly lower actual volumes of particles delivered intra-articularly. Since particles were *in vivo* for a period of seven days, and were introduced via an injection, particles produced by a prosthesis may have differing particle aggregation and protein corona characteristics, though it has been suggested that a hard protein corona is formed after just 48 h [52]. In addition, particles may not have dispersed as they would in an *in vivo* scenario where particles are continuously produced. It is also possible that there were subtle changes to particle geometries

that could not be detected due to the resolution limit of the SEM equipment; however, international guidelines for minimum magnifications were followed [26,35]. The measurements of the particles were also limited due to their aggregated nature, which meant that manual particle sizing was required. This limited the number of particles that it was feasible to size, though international guidelines were also followed with regard to minimum particle numbers for statistical analysis of particle characteristics. Another possible limitation of the current study is that during elemental analysis of isolated particles, tungsten was identified on CoCrMo particles. However, this had no detectable effect on particle size or morphology and the tungsten could likely be removed by further rounds of ultracentrifugation, as described in the washing stages of the protocol. Furthermore, elemental analysis demonstrated a lack of any other contaminating elements on particles, suggesting that particles were relatively pure.

5. Conclusion

The isolation technique reported here represents an improvement to current particle isolation methods from tissue, due to its more effective removal of proteins and greater sensitivity. This work could be valuable to future animal and explant studies evaluating ceramic or metal particles, especially as the latest generation of orthopaedic materials are highly wear-resistant, and thus there may be a need to isolate increasingly lower volumes of particles.

Acknowledgements

The research leading to these results has received funding from the European Union's Seventh Framework Programme (FP7/2007-2013) under grant agreement no. GA-310477, LifeLongJoints.

The authors acknowledge Pat Campbell, PhD, for her advice and earlier work on particle isolation, and Stuart Micklethwaite, for his support using the facilities at the Leeds Electron Microscopy and Spectroscopy centre.

References

[1] NJR. 13th Annual Report. 2016.
[2] Khosla S. Minireview, The OPG/RANKL/RANK system, Endocrinology 142 (2001) 5050–5055.
[3] B. Baumann, C.P. Rader, J. Seufert, U. Noth, O. Rolf, J. Eulert, F. Jakob, Effects of polyethylene and TiAlV wear particles on expression of RANK, RANKL and OPG mRNA, Acta Orthop. Scand. 75 (2004) 295–302.
[4] B.H. Bosker, H.B. Ettema, M.F. Boomsma, B.J. Kollen, M. Maas, C.C.P.M. Verheyen, High incidence of pseudotumour formation after large-diameter metal-on-metal total hip replacement a prospective cohort study, J. Bone Joint Surg. Br. 94B (2012) 755–761.
[5] FDA, Use of International Standard ISO 10993-1, "Biological evaluation of medical devices – Part 1: Evaluation and testing within a risk management process", Guidance for Industry and Food and Drug Administration Staff, in: FDA (Ed.), 2016.
[6] M.J. Nine, D. Choudhury, A.C. Hee, R. Mootanah, N.A. Abu Osman, Wear Debris characterization and corresponding biological response: artificial hip and knee joints, Materials 7 (2014) 980–1016.
[7] P. Campbell, S. Ma, B. Yeom, H. Mckellop, T.P. Schmalzried, H.C. Amstutz, Isolation of predominantly submicron-sized Uhmwpe wear particles from periprosthetic tissues, J. Biomed. Mater. Res. 29 (1995) 127–131.
[8] A. Kobayashi, W. Bonfield, Y. Kadoya, T. Yamac, M.A.R. Freeman, G. Scott, P.A. Revell, The size and shape of particulate polyethylene wear debris in total joint replacements, Proc. Inst. Mech. Eng. H 211 (1997) 11–15.
[9] J.D. Mabrey, A. Afsar-Keshmiri, G.A. Engh, C.J. Sychterz, M.A. Wirth, C.A. Rockwood, C.M. Agrawal, Standardized analysis of UHMWPE wear particles from failed total joint arthroplasties, J. Biomed. Mater. Res. 63 (2002) 475–483.
[10] D.W. Hahn, D.L. Wolfarth, N.L. Parks, Analysis of polyethylene wear debris using micro-Raman spectroscopy: a report on the presence of beta-carotene, J. Biomed. Mater. Res. 35 (1997) 31–37.
[11] D.L. Wolfarth, D.W. Han, G. Bushar, N.L. Parks, Separation and characterization of polyethylene wear debris from synovial fluid and tissue samples of revised knee replacements, J. Biomed. Mater. Res. 34 (1997) 57–61.
[12] A.S. Shanbhag, J.J. Jacobs, T.T. Glant, J.L. Gilbert, J. Black, J.O. Galante, Composition and morphology of wear debris in failed uncemented total hip-replacement, J. Bone Joint Surg. Br. 76B (1994) 60–67.
[13] J.L. Tipper, E. Ingham, J.L. Hailey, A.A. Besong, J. Fisher, B.M. Wroblewski, M.H. Stone, Quantitative analysis of polyethylene wear debris, wear rate and head damage in retrieved Charnley hip prostheses, J. Mater. Sci.-Mater. M 11 (1999) 117–124.
[14] G.I. Howling, P.I. Barnett, J.L. Tipper, M.H. Stone, J. Fisher, E. Ingham, Quantitative characterization of polyethylene debris isolated from periprosthetic tissue in early failure knee implants and early and late failure Charnley hip implants, J. Biomed. Mater. Res. 58 (2001) 415–420.
[15] K.J. Margevicius, T.W. Bauer, J.T. Mcmahon, S.A. Brown, K. Merritt, Isolation and characterization of debris in membranes around total joint prostheses, J. Bone Joint Surg. Am. 76A (1994) 1664–1675.
[16] M. Slouf, S. Eklova, J. Kumstatova, S. Berger, H. Synkova, A. Sosna, D. Pokorny, M. Spundova, G. Entlicher, Isolation, characterization and quantification of polyethylene wear debris from periprosthetic tissues around total joint replacements, Wear 262 (2007) 1171–1181.
[17] K. Hirakawa, T.W. Bauer, B.N. Stulberg, A.H. Wilde, M. Secic, Characterization and comparison of wear debris from failed total hip implants of different types, J. Bone Joint Surg. Am. 78A (1996) 1235–1243.
[18] S. Lerouge, O. Huk, L.H. Yahia, L. Sedel, Characterization of in vivo wear debris from ceramic-ceramic total hip arthroplasties, J. Biomed. Mater. Res. 32 (1996) 627–633.
[19] M. Bohler, Y. Mochida, T.W. Bauer, H. Plenk, M. Salzer, Wear debris from two different alumina-on-alumina total hip arthroplasties, J. Bone Joint Surg. Br. 82B (2000) 901–909.
[20] Y. Mochida, M. Boehler, M. Salzer, T.W. Bauer, Debris from failed ceramic-on-ceramic and ceramic-on-polyethylene hip prostheses, Clin. orthopaedics Related Res. (2001) 113–125.
[21] R.M. Baxter, M.J. Steinbeck, J.L. Tipper, J. Parvizi, M. Marcolongo, S.M. Kurtz, Comparison of periprosthetic tissue digestion methods for ultra-high molecular weight polyethylene wear debris extraction, J. Biomed. Mater. Res. B 91B (2009) 409–418.
[22] I. Catelas, J.D. Bobyn, J.J. Medley, D.J. Zukor, A. Petit, O.L. Huk, Effects of digestion protocols on the isolation and characterization of metal-metal wear particles. II. analysis of ion release and particle composition, J. Biomed. Mater. Res. 55 (2001) 330–337.
[23] P.F. Doorn, P.A. Campbell, J. Worrall, P.D. Benya, H.A. McKellop, H.C. Amstutz, Metal wear particle characterization from metal on metal total hip replacements: transmission electron microscopy study of periprosthetic tissues and isolated particles, J. Biomed. Mater. Res. 42 (1998) 103–111.
[24] C. Brown, S. Williams, J.L. Tipper, J. Fisher, E. Ingham, Characterisation of wear particles produced by metal on metal and ceramic on metal hip prostheses under standard and microseparation simulation, J. Mater. Sci.-Mater. M 18 (2007) 819–827.
[25] I. Milosev, M. Remskar, In vivo production of nanosized metal wear debris formed by tribochemical reaction as confirmed by high-resolution TEM and XPS analyses, J. Biomed. Mater. Res. A 91A (2009) 1100–1110.
[26] ISO 17853, Wear of Implant Materials – Polymer and Metal Wear Particles – Isolation and Characterization, ISO, Geneva, Switzerland, 2011.
[27] F. Billi, P. Benya, A. Kavanaugh, J. Adams, H. McKellop, E. Ebramzadeh, The John Charnley award: an accurate and extremely sensitive method to separate, display, and characterize wear debris part 2: metal and ceramic particles, Clin. Orthopaedics Related Res. 470 (2012) 339–350.
[28] S. Lal, R.M. Hall, J.L. Tipper, A novel method for isolation and recovery of ceramic nanoparticles and metal wear debris from serum lubricants at ultra-low wear rates, Acta Biomater. 42 (2016) 420–428.
[29] M.A. Germain, A. Hatton, S. Williams, J.B. Matthews, M.H. Stone, J. Fisher, E. Ingham, Comparison of the cytotoxicity of clinically relevant cobalt-chromium and alumina ceramic wear particles in vitro, Biomaterials 24 (2003) 469–479.
[30] EU, Directive 2010/63/EU of The European Parliament and of the council of 22 on the protection of animals used for scientific purposes, Off. J. Eur. Union 2010 (September 2010) 33–79.
[31] ASTM F1537, Standard Specification for Wrought Cobalt-28Chromium-6Molybdenum Alloys for Surgical Implants, ASTM International, West Conshohocken, PA, 2011.
[32] J. Patel, S. Lal, S.P. Wilshaw, R.M. Hall, J.L. Tipper, Recovery rate of particle isolation using sodium polytungstate density gradients, Data in Brief, 2017, Under review.
[33] J. Patel, S. Lal, S.P. Wilshaw, R.M. Hall, J.L. Tipper, Development and optimisation of a tissue digestion method for the isolation of orthopaedic wear particles, Data in Brief, 2017, Under review.
[34] J. Patel, S. Lal, S.P. Wilshaw, R.M. Hall, J.L. Tipper, Validation of a novel particle isolation procedure using particle doped tissue samples, Data in Brief, 2017, Under review.
[35] ASTM F1877, Standard Practice for Characterization of Particles, ASTM International, West Conshohocken, PA, 2016.
[36] E. Ingham, J. Fisher, M. Stone, Wear of historical polyethylenes in hip prostheses. Biomechanical success and a biological failure, Hip Int. 13 (2003) S17–S27.
[37] J.E. Nevelos, E. Ingham, C. Doyle, J. Fisher, A.B. Nevelos, Analysis of retrieved alumina ceramic components from Mittelmeier total hip prostheses, Biomaterials 20 (1999) 1833–1840.

[38] A. Hatton, J.E. Nevelos, J.B. Matthews, J. Fisher, E. Ingham, Effects of clinically relevant alumina ceramic wear particles on TNF-alpha production by human peripheral blood mononuclear phagocytes, Biomaterials 24 (2003) 1193–1204.
[39] C. Brown, L. Lacharme-Lora, B. Mukonoweshuro, A. Sood, R.B. Newson, J. Fisher, C.P. Case, E. Ingham, Consequences of exposure to peri-articular injections of micro- and nano-particulate cobalt-chromium alloy, Biomaterials 34 (2013) 8564–8580.
[40] C. Esposito, F. Maclean, P. Campbell, W.L. Walter, W.K. Walter, S.F. Bonar, Periprosthetic tissues from third generation alumina-on-alumina total hip arthroplasties, J. Arthroplasty 28 (2013) 860–866.
[41] T. Takeichi, O. Kitamura, Detection of diatom in formalin-fixed tissue by proteinase K digestion, Forensic Sci. Int. 190 (2009) 19–23.
[42] I. Catelas, J.D. Bobyn, J.B. Medley, J.J. Krygier, D.J. Zukor, O.L. Huk, Size, shape, and composition of wear particles from metal-metal hip simulator testing: effects of alloy and number of loading cycles, J. Biomed. Mater. Res. A 67A (2003) 312–327.
[43] P. Aggarwal, J.B. Hall, C.B. McLeland, M.A. Dobrovolskaia, S.E. McNeil, Nanoparticle interaction with plasma proteins as it relates to particle biodistribution, biocompatibility and therapeutic efficacy, Adv. Drug Delivery Rev. 61 (2009) 428–437.
[44] J.L. Tipper, P.J. Firkins, A.A. Besong, P.S.M. Barbour, J. Nevelos, M.H. Stone, E. Ingham, J. Fisher, Characterisation of wear debris from UHMWPE on zirconia ceramic, metal-on-metal and alumina ceramic-on-ceramic hip prostheses generated in a physiological anatomical hip joint simulator, Wear 250 (2001) 120–128.
[45] P.J. Firkins, J.L. Tipper, M.R. Saadatzadeh, E. Ingham, M.H. Stone, R. Farrar, J. Fisher, Quantitative analysis of wear and wear debris from metal-on-metal hip prostheses tested In a physiological hip joint simulator, Bio-Med. Mater. Eng. 11 (2001) 143–157.
[46] S. Grosse, H.K. Haugland, P. Lilleng, P. Ellison, G. Hallan, P.J. Hol, Wear particles and ions from cemented and uncemented titanium-based hip prostheses-a histological and chemical analysis of retrieval material, J. Biomed. Mater. Res. B 103 (2015) 709–717.
[47] M. Pettersson, C. Skjoldebrand, L. Filho, H. Engqvist, C. Persson, Morphology and dissolution rate of wear debris from silicon nitride coatings, ACS Biomater. Sci. Eng. 2 (2016) 998–1004.
[48] A.Q. Liu, L. Richards, C.L. Bladen, E. Ingham, J. Fisher, J.L. Tipper, The biological response to nanometre-sized polymer particles, Acta Biomater. 23 (2015) 38–51.
[49] B.D. Chithrani, A.A. Ghazani, W.C.W. Chan, Determining the size and shape dependence of gold nanoparticle uptake into mammalian cells, Nano Lett. 6 (2006) 662–668.
[50] S.Y. Yang, W.P. Ren, Y.S. Park, A. Sieving, S. Hsu, S. Nasser, P.H. Wooley, Diverse cellular and apoptotic responses to variant shapes of UHMWPE particles in a murine model of inflammation, Biomaterials 23 (2002) 3535–3543.
[51] Z.Q. Chu, S.L. Zhang, B.K. Zhang, C.Y. Zhang, C.Y. Fang, I. Rehor, P. Cigler, H.C. Chang, G. Lin, R.B. Liu, Q. Li, Unambiguous observation of shape effects on cellular fate of nanoparticles, Sci. Rep. 4 (2014).
[52] E. Casals, T. Pfaller, A. Duschl, G.J. Oostingh, V. Puntes, Time evolution of the nanoparticle protein corona, ACS Nano 4 (2010) 3623–3632.